Ozone pollution mitigation strategy informed by long-term trends of atmospheric oxidation capacity

Wenjie Wang[1,2,3], Xin Li[1,4,5,6]*, Yafang Cheng[2], David D. Parrish[7], Ruijing Ni[2], Zhaofeng Tan[8,4], Ying Liu[1,4,5], Sihua Lu[1,4,5], Yusheng Wu[1,†], Shiyi Chen[1,4,5], Keding Lu[1,4,5,6], Min Hu[1,4,5,6], Limin Zeng[1,4,5], Min Shao[1,7], Cheng Huang[9], Xudong Tian[10], K. M. Leung[11], Liangfu Chen[12], Meng Fan[12], Qiang Zhang[13], Franz Rohrer[8,4], Andreas Wahner[8,4], Ulrich Pöschl[2], Hang Su[3,9,2]*, Yuanhang Zhang[1,4,5,6]*

[1] State Key Joint Laboratory of Environmental Simulation and Pollution Control, College of Environmental Sciences and Engineering, Peking University, Beijing, 100871, China.

[2] Max Planck Institute for Chemistry, Mainz, 55128, Germany.

[3] Institute of Atmospheric Physics, Chinese Academy of Sciences, Beijing, 310012, China.

[4] International Joint Laboratory for Regional Pollution Control, Ministry of Education, Beijing, 100816, China.

[5] Collaborative Innovation Centre of Atmospheric Environment and Equipment Technology, Nanjing University of Information Science & Technology, Nanjing, 210044, China.

[6] Institute of Carbon Neutrality, Peking University, Beijing, 100871, China.

[7] Institute for Environmental and Climate Research, Jinan University, Guangzhou, 511443, China.

[8] Institut für Energie-und Klimaforschung: Troposphäre (IEK-8), Forschungszentrum Jülich, Jülich, 52428, Germany.

[9] State Environmental Protection Key Laboratory of Formation and Prevention of Urban Air Pollution Complex, Shanghai Academy of Environmental Sciences, Shanghai, 200233, China.

[10] Key Laboratory of Ecological and Environmental Monitoring, Forewarning and Quality Control of Zhejiang, Zhejiang Ecological and Environmental Monitoring

Center, Hangzhou, 310012, China.

[11] Environmental Protection Department, The Government of the Hong Kong Special Administrative Region, Hong Kong, China.

[12] State Key Laboratory of Remote Sensing Science, The Aerospace Information Research Institute, Chinese Academy of Sciences, 100101 Beijing, China

[13] Department of Earth System Science, Tsinghua University, 100084 Beijing, China

[†] now at: Department of Physics, University of Helsinki, Helsinki, 00560, Finland

* To whom correspondence should be addressed.

Email: li_xin@pku.edu.cn (X. L.), h.su@mpic.de (H. S.), yhzhang@pku.edu.cn (Y. H. Z.)

Abstract: Tropospheric ozone pollution is a critical air quality concern in China. However, the most effective mitigation approach remains unclear, with prioritizing the reduction of volatile organic compounds or nitrogen oxides (NO_X) currently still under debate. Here, we analyze observational measurements of ozone in August, and its precursors, from urban Beijing between 2006 and 2020. We show that despite a continuous increase of the primary atmospheric oxidant (hydroxyl radical, OH), ozone increased until 2014 and then decreased. This ozone trend can be explained by changes in OH turnover rate, primarily determined by the reactivity ratio between volatile organic compounds and NO_X. Overall, reactive abatement of volatile organic compounds should be a near-future priority for ozone pollution control in China, followed by further NO_X controls.

During past decades China experienced rapid industrialization, which brought economic advantages, but also caused significantly deteriorated air quality [1, 2]. According to WHO guidelines, ozone (O_3) and fine particulate matter with a diameter of less than 2.5 micrometers ($PM_{2.5}$) are the chief hazards of China's air pollution [3]. Over the past decade, China launched the toughest-ever clean air policy in the country [4]. These efforts, by reducing emissions of primary pollutants such as VOCs, NO_X, SO_2 and others, improved $PM_{2.5}$ air quality [4, 5]. However, O_3 continued to increase and only began to stabilize at a later stage [2, 6]. This contrasts with the generally decreasing O_3 trend in Europe and North America due to continuous reductions of VOCs and NO_X emissions since the 1990s [7, 8, 9, 10]. The causes of the contrasting trends and adverse O_3 pollution trends in China are still not well understood, representing a grand challenge for O_3 pollution control and development of effective strategies for continued air quality improvement. Several studies have devoted efforts to explore the causes of rising O_3 levels in Beijing, a typical megacity in China. Wang and Zhang et al reported that the local photochemistry driven by VOCs and NO_X emissions plays a vital role in determining O_3 trend in the city [11, 12, 13]. Other research has evaluated the impact of meteorological variability on the long-term trend of O_3 in Beijing [14, 15], showing a minor effect of meteorological variability compared to variations in anthropogenic emissions.

Tropospheric O_3 is directly produced from photolysis of nitrogen dioxide (NO_2). NO_2 can be produced during the gas-phase oxidation of NO by peroxyl radicals, which are produced from the oxidation of VOCs by hydroxyl (OH) radicals [16]. We demonstrate that the dependence of OH radical cycling on ambient NO_X and VOCs

concentrations is key to understanding the O_3 trend in China and the contrast in O_3 trends between China and other regions.

Trends of O_3 and its precursors in Beijing

Beijing is one of the megacities in China, suffering from severe O_3 pollution. The implementation of emission reductions in Beijing began earlier and has been more stringent than in other cities in China [17], which provides a good opportunity to study the response of O_3 pollution to precursors' abatements from a long-term perspective. The experience of Beijing can serve as a model for other cities in China that still suffer from rapidly increasing O_3. This study is based on August measurements in Beijing from 2006 to 2020, which is the most comprehensive, long-term observational data set of O_3 and its precursors VOCs and NO_X that is available in China (Methods M1; Extended data Table 1). Although the O_3 concentrations in August are not the highest in summer, they are not much different from other months of the O_3 pollution season (May to August) (Extended data Fig. 1). The highest O_3 concentration occurred in June and July with mean maximum daily 8-hour average (MDA8) O_3 concentration of 80 ppbv during 2014-2020, which is higher than that in August by 9 ppbv.

Given that variations in meteorological and other physical conditions can affect O_3 trends, we use a multiple linear regression method to remove the impact of photolysis frequencies, temperature, relative humidity, wind speed and wind direction on O_3, thereby obtaining a normalized O_3 (Methods M2) [18, 19]. Figure 1B shows that mean MDA8 O_3 concentrations in August increased before 2014, and then decreased in

the following years. The normalized O_3 also shows a non-monotonic trend, with a smaller increase before 2014, compared to the mean MDA8 O_3 concentrations (Fig. 1D). Similar variable trends are also found for other secondary oxidation products such as formaldehyde (Extended data Fig. 2).

Figure 1A shows the changes in OH reactivity of NO_X and VOCs (NO_X^R and VOC^R) based on August measurements in Beijing from 2006 to 2020. NO_X^R and VOC^R are defined as the concentration of NO_X and VOCs multiplied by their respective reaction rate coefficients with OH (CO is included in the calculation of VOC^R as detailed in Supplementary S2). Both NO_X^R and VOC^R show consistently decreasing trends, confirming the effects of emission controls reported in earlier studies [4, 20]. Clearly, the trend of O_3 precursors is distinct from that of O_3.

To understand the relationship between OH radical cycling and the O_3 trend, we first investigate the ratio VOC^R/NO_X^R where VOC^R and NOx^R represent the main production and sink terms of OH radicals, respectively [21, 22]. VOC^R acts as a production term because the reaction of VOCs with OH produces peroxyl radicals and oxygenated VOCs (OVOCs) which will increase OH through recycling and amplification of OH [23, 24]. It is notable that the trend of VOC^R/NO_X^R (Fig. 1C) is similar to that of normalized O_3; both remained approximately constant before 2014, and then decreased rapidly after 2014. The rapid decrease in VOC^R/NO_X^R after 2014 is attributed to decreases in industrial emissions with high emission ratios of VOC to NO_X and in solvent usage [17] under the more rigorous emissions standards implemented during the clean air action plan in 2013-2020 [4, 20]. As shown in Fig. 1A, compared to an almost constant decreasing

trend of NO_X^R (-3.4% yr^{-1}, r^2=0.66), VOC^R decreased faster after 2014 (-7.6% yr^{-1}, r^2=0.68) than before 2014 (-3.0% yr^{-1}, r^2=0.45). In addition to Beijing, the similarity of trends between VOC^R/NO_X^R and normalized O_3 is also seen in other Chinese urban areas such as Shanghai in the Yangtze River Delta and Hong Kong in the Pearl River Delta (Extended data Fig. 3); however, in contrast to Beijing these two variables have consistently increased in Shanghai from 2011 to 2019 and in Hong Kong from 2013 to 2019, rather than showing recent decreases.

The relationship between OH radical cycling and the O_3 trend

To gain a deeper insight, we investigated the detailed radical cycling and photochemistry by applying an advanced box model based on the updated Master Chemical Mechanism v3.3 chemistry scheme (MCM 3.3) [25]. This model is constrained by the comprehensive observations and accounts for the diurnal evolution of the planetary boundary layer [26] and heterogeneous uptake of HO_2 radicals and reactive nitrogen species onto aerosols (Methods M3). The model accurately simulates the observed O_3 (Fig. 1B), OH (Fig. S7) and other photochemical products (Fig. S6 and Fig. S10) with biases smaller than 20%.

The box model simulation shows that OH increased continuously during 2006-2020, giving an approximate doubling (Fig. 2A). Besides the box model simulations, we have also adopted another approach, using a measurable proxy, the ratio of daytime methyl vinyl ketone plus methacrolein (MVK+MACR) to isoprene [27, 28] which is approximately proportional to the OH concentration (Supplementary S5), to represent

the OH trend. As shown in Fig. 2A, the observed and simulated (MVK+MACR)/isoprene agree, and display an increasing trend from 2010 to 2020, providing strong support for the modeled OH trend. To identify the primary causes of the continuous OH increase, we performed sensitivity analyses of the relevant factors. The main drivers of the OH change are the increase of photolysis frequencies[29], decrease in NO_X emissions, decrease in VOC emissions, and reduced heterogeneous uptake [30], which leads to relative changes of +44%, +56%, -23% and +15%, respectively (Fig. 2B). As the photochemical conditions over this period (2006 to 2020) were always in the NO_X-saturated regime (Methods M4), NO_X reduction increased OH, and VOC reduction decreased OH (Extended data Fig. 4). The combined effect of other factors (including the changes in O_3, H_2O and temperature) played only a minor role in the OH budget change.

Given the trend of OH radicals, we can approximate the ozone production rate $P(O_3)$ by Eq (1) and Eq (2), as detailed in Methods M4:

$$P(\mathrm{O_3}) = \alpha k_{HO2+NO}[\mathrm{HO_2}][\mathrm{NO}] \quad (1)$$

$$\alpha k_{HO2+NO}[\mathrm{HO_2}][\mathrm{NO}] = \alpha k_{OH+VOC}[\mathrm{OH}][\mathrm{VOC}] = \alpha[\mathrm{OH}]\mathrm{VOC^R} \quad (2)$$

where the coefficient α is equal to $([RO_2]+[HO_2])/[HO_2]$, which remained approximately constant over the 2006-2020 period according to the model output (Methods M4). Equation (2) holds under conditions when the radical chain cycling is much more important than chain initiation [22, 31]; these conditions are established in Beijing (Methods M4; Extended data Fig. 5).

Figure 2C shows the trend of O_3 production calculated from the OH turnover rate

190 induced by VOCs ([OH]×VOC^R) according to Eq (2). Consistent with the trend of
191 observed O_3 concentrations (Fig. 1B), [OH]×VOC^R also shows two distinct trends,
192 increasing before 2014 and decreasing after 2014. The strong positive correlation of
193 [OH]×VOC^R with O_3 and O_X (O_X=O_3+NO_2) concentrations (Fig. 2D) also demonstrates
194 that the change of ambient O_3 over the entire 2006 to 2020 period is consistent with our
195 understanding of O_3 photochemistry and OH cycling. Given that O_3 production
196 primarily depends on [OH]×VOC^R, the contrasting O_3 trends before and after 2014 can
197 be explained by a reduction in VOC^R that was smaller than the increase in OH before
198 2014, but larger after 2014.

199 Figures 1 and 2 show that by affecting OH cycling, VOC^R/NO_X^R controls the
200 trends of $P(O_3)$ and O_3 concentration. The underlying mechanisms, however, remain
201 under debate. A key parameter here is the radical chain length (ChL), defined as
202 $\alpha k_{HO2+NO}[HO_2][NO]/P(RO_X)$, which characterizes the average number of cycles each
203 RO_X radical makes prior to termination. Tonnesen and Dennis [32] suggested that the
204 effect of VOC/NO_X on $P(O_3)$ changes is mainly through changing the ChL, while
205 several studies suggested its effects are mainly on primary production of RO_X
206 (RO_X=OH+HO_2+RO_2) radicals ($P(RO_X)$) [23, 33]. $P(RO_X)$ has contributions from the
207 photolysis of radical precursors (including carbonyls, nitrous acid and O_3) and alkene
208 ozonolysis (Methods M4). ChL primarily depends on the levels of VOCs and NO_X[34].

209 To elucidate the actual mechanism in Beijing, we investigated the effects of both
210 ChL and $P(RO_X)$ as shown in Eq (3), where $P(O_3)$ is expressed as the product of $P(RO_X)$
211 and ChL:

$$P(O_3) = P(RO_X) \times ChL \quad (3)$$

As shown in Fig. 3A, the $P(RO_X)$ increased only slightly before 2014 but decreased after 2014 with a trend similar to that of $[OH] \times VOC^R$ (i.e., $P(O_3)$), while the ChL level remained stable with no significant change. This is clear evidence that in Beijing it is the change of $P(RO_X)$ rather than ChL that controls the distinct trends of O_3 production before and after 2014. Among the different contributors to $P(RO_X)$, photolysis of oxygenated VOCs (OVOCs) was the largest contributor (Fig. 3B). Both measurements and model simulations show a strong dependence of OH reactivity of OVOCs ($OVOC^R$) on VOC^R/NO_X^R (Fig. 3C**)**. The decreasing VOC^R/NO_X^R after 2014 (Fig. 1C) weakened OH radical cycling, resulting in a decrease in the production of OVOCs, which in turn reduced $P(RO_X)$ to further reduce the production of O_3 (Fig. 3D). Note that reduction of VOCs also contributed to the reduction of OVOCs but is less important than the reduction of VOC^R/NO_X^R. The source apportionment of OVOCs indicates that reductions in primary emissions and secondary production contribute 28% and 70% of the reduction in the $OVOC^R$, respectively (Supplementary S6).

O_3 mitigation strategy for Chinese cities

Figure 4 shows the combined effect of VOCs and NO_X on normalized O_3 and total OH turnover rate induced by all reactive gases (including VOCs, NO_X and SO_2). The total OH turnover rate is the total reaction rate of all reactive species with OH radical, which closely relates to the level of secondary pollution (Methods M4). The Beijing environment during 2006-2020 was overall in the VOC-limited regime for both O_3 and

total OH turnover rate, with a trend of moving toward to the transition regime (between VOC-limited and NO_X-limited regimes). The O_3 trend line parallels the isopleths before 2014, followed by efficiently decreasing O_3 after 2014 (Fig. 4A**)**, which is consistent with the observed trend of normalized O_3 as shown in Fig. 1D. Figure 4 clearly shows that the turning point of the O_3 trend appears in 2014 due to a faster decrease in VOC^R/NO_X^R after 2014 than before 2014.

If VOCs and NO_X in Beijing maintain their current declining trends over the next five years (blue lines from 2020 to 2025 in Fig. 4), both O_3 and total OH turnover rate will continue to decrease. By 2025 anthropogenic VOCs will have decreased to a very low level and biogenic VOCs will dominate the total VOCs reactivity, which means that further reduction of anthropogenic VOCs may have little impact on VOC^R/NO_X^R. Moreover, in 2025, the O_3 production will have moved to a transition regime. In this case, a faster NO_X reduction after 2025 will help O_3 production rapidly enter a NO_X-limited regime, which favors O_3 mitigation through further reducing NO_X (magenta lines after 2025 in Fig. 4). The situation in Shanghai (Extended data Fig. 6) is similar to that in Beijing. In addition to the two largest cities, most urban regions in China have been changing from a VOC-limited regime to a transition regime [35, 36]. These findings suggest that priority on VOCs abatement in the short term, followed by NO_X abatement in the long term is the optimal strategy for summertime O_3 air quality improvement in Chinese cities.

Acknowledgements

X. L. received financial support of the National Natural Science Foundation of China (91644108, 91844301). X. L. received financial support of the Beijing Municipal Natural Science Fund for Distinguished Young Scholars (grant No. JQ21030). F. R. and A. W. received financial support of the Federal Ministry of Education and Research, Germany (01LP1929A, Practice). H. S. received financial support of the National Key Scientific and Technological Infrastructure project "Earth System Numerical Simulation Facility" (EarthLab).

Author contributions statement

H. S., X. L., Y. Z., and Y. C. conceived, and designed this study, and revised the article critically. W. W. and X. L. acquired, analyzed, and interpreted data, drafted the article, and revised it critically. R. N. and Y. C. performed the chemical transport model simulations. D. D. P., F. R., A. W., R. N., Z. T. and U. P. revised the article critically. Q. Z. provided the emission inventory data. Y. L., S. L., Y. W., S. C., K. L., M. H., L. Z., M. S., C. H., X. T., K. M. L., L. C., M. F. collected data.

Competing interest statement

Authors declare no competing interests.

Figure Legends

Figure 1. Variations in ozone and OH reactivity of precursors derived from observations in Beijing, August between 2006 and 2020. Variations in daytime (6:00-19:00) averages of VOC^R (including primary hydrocarbons plus carbon monoxide), NO_X^R and column concentrations of NO_2 (A), MDA8 O_3 concentrations (B), the ratio of VOC^R to NO_X^R (C), and normalized MDA8 O_3 concentrations (D). Dashed lines show linear regression fits to observations in periods before and after 2014. Model-simulated MDA8 O_3 concentrations are included in (B).

Figure 2. Variations in model-simulated OH concentrations and its driving forces in Beijing. (A) Variations in simulated daytime average OH concentrations (red dots) and measured and simulated (MVK+MACR)/isoprene ratios (blue dots and circles) in Beijing in August between 2006 and 2020. Dashed lines show exponential regression fits to trends. (B) Apportionment of the causes of the change in OH derived from box model sensitivity analysis. (C) Variations in OH turnover rate induced by VOCs ($OH \times VOC^R$). Dashed lines show linear regression fits to trends in periods before and after 2014. (D) Correlation of $OH \times VOC^R$ with observed MDA8 O_3 and daytime O_X concentrations.

Figure 3. The impact of the VOC^R/NO_X^R ratio on ozone production. (A) Variations

in P(RO_X) and ChL. The three metrics are colored by the VOC^R/NO_X^R ratio. (B) Hourly mean diurnal profiles of modeled rates of primary RO_X production during 2006-2020. (C) Modeled (circle dots) and observed (black diamonds) dependence of $OVOC^R$ on VOC^R/NO_X^R ratio. The modeled results are colored by different VOC^R levels. The observed results indicate mean values of $OVOC^R$ with standard deviations at each VOC^R/NO_X^R range, with sample size of 132 daily average values in total. (D) Mechanism diagram showing the impact of decreased VOC^R/NO_X^R ratio on ozone production.

Figure 4. Isopleth plots for (A) ozone and (B) total OH turnover rate as a function of NO_X^R and VOC^R. Red solid circles represent the average levels of MDA8 O_3 and daytime OH turnover rate for each year during 2006-2020, and the solid lines indicate fits to the trends during 2006-2014 and 2014-2020. The yellow dotted lines indicate the VOC^R level from biogenic emissions. The blue and magenta arrows indicate future routes for VOCs and NO_X abatement that mitigate ozone effectively in the short term (2020-2025) and long term (after 2025), respectively.

References:

1. Huang RJ, Zhang YL, Bozzetti C, Ho KF, Cao JJ, Han YM*, et al.* High secondary aerosol contribution to particulate pollution during haze events in China. *Nature* 2014, **514**(7521)**:** 218-222.
2. Lu X, Hong JY, Zhang L, Cooper OR, Schultz MG, Xu XB*, et al.* Severe Surface Ozone Pollution in China: A Global Perspective. *Environ Sci Technol Lett* 2018, **5**(8)**:** 487-494.
3. World Health Organization (WHO), WHO global air quality guidelines: particulate matter (PM2.5 and PM10), ozone, nitrogen dioxide, sulfur dioxide and carbon monoxide: executive summary. Publication ISBN: 978-92-4-003443-3, WHO, 2021 https://apps.who.int/iris/bitstream/handle/10665/345334/9789240034433-eng.pdf.
4. Zhang Q, Zheng Y, Tong D, Shao M, Wang S, Zhang Y*, et al.* Drivers of improved PM2.5 air quality in China from 2013 to 2017. *Proc National Acad Sci* 2019, **116**(49)**:** 24463-24469.
5. Wang S, Su H, Chen C, Tao W, Streets DG, Lu Z*, et al.* Natural gas shortages during the "coal-to-gas" transition in China have caused a large redistribution of air pollution in winter 2017. *Proc National Acad Sci* 2020, **117**(49)**:** 31018-31025.
6. Lu X, Zhang L, Wang X, Gao M, Li K, Zhang Y*, et al.* Rapid increases in warm-season surface ozone and resulting health impact in China since 2013. *Environ Sci Technol Lett* 2020, **7**(4)**:** 240-247.
7. Fiore AM, Jacob DJ, Logan JA, Yin JH. Long-term trends in ground level ozone

over the contiguous United States, 1980–1995. *J Geophys Res-Atmos* 1998, **103**(D1)**:** 1471-1480.

8. Cooper OR, Parrish D, Ziemke J, Balashov N, Cupeiro M, Galbally I*, et al.* Global distribution and trends of tropospheric ozone: An observation-based reviewGlobal distribution and trends of tropospheric ozone. *Elem Sci Anth* 2014, **2:** 29.
9. Simon H, Reff A, Wells B, Xing J, Frank N. Ozone Trends Across the United States over a Period of Decreasing NOx and VOC Emissions. *Environ Sci Technol* 2015, **49**(1)**:** 186-195.
10. Fleming ZL, Doherty RM, Von Schneidemesser E, Malley CS, Cooper OR, Pinto JP*, et al.* Tropospheric Ozone Assessment Report: Present-day ozone distribution and trends relevant to human health. *Elem Sci Anth* 2018, **6:** 12.
11. Wang W, Parrish DD, Li X, Shao M, Liu Y, Mo Z*, et al.* Exploring the drivers of the increased ozone production in Beijing in summertime during 2005–2016. *Atmos Chem Phys* 2020, **20**(24)**:** 15617-15633.
12. Zhang Q, Yuan B, Shao M, Wang X, Lu S, Lu K*, et al.* Variations of ground-level O3 and its precursors in Beijing in summertime between 2005 and 2011. *Atmos Chem Phys* 2014, **14**(12)**:** 6089-6101.
13. Liu Y, Wang T. Worsening urban ozone pollution in China from 2013 to 2017 – Part 2: The effects of emission changes and implications for multi-pollutant control. *Atmos Chem Phys* 2020, **20**(11)**:** 6323-6337.
14. Cheng N, Li R, Xu C, Chen Z, Chen D, Meng F*, et al.* Ground ozone variations at

364 an urban and a rural station in Beijing from 2006 to 2017: Trend, meteorological
365 influences and formation regimes. *Journal of Cleaner Production* 2019, **235:** 11-20.
366 15. Ma ZQ, Xu J, Quan WJ, Zhang ZY, Lin WL, Xu XB. Significant increase of surface
367 ozone at a rural site, north of eastern China. *Atmos Chem Phys* 2016, **16**(6)**:** 3969-
368 3977.
369 16. Monks PS, Archibald A, Colette A, Cooper O, Coyle M, Derwent R, *et al.*
370 Tropospheric ozone and its precursors from the urban to the global scale from air
371 quality to short-lived climate forcer. *Atmos Chem Phys* 2015, **15**(15)**:** 8889-8973.
372 17. UN Environment. A review of 20 years' air pollution control in Beijing. Publication
373 ISBN: 978-92-807-3743-1, United Nations Environment Programme, 2019,
374 https://wedocs.unep.org/bitstream/handle/20.500.11822/27645/airPolCh_EN.pdf?s
375 equence=1&isAllowed=y.
376 18. Yang Y, Liao H, Lou S. Increase in winter haze over eastern China in recent decades:
377 Roles of variations in meteorological parameters and anthropogenic emissions. *J*
378 *Geophys Res-Atmos* 2016, **121**(21)**:** 13,050-013,065.
379 19. Li K, Jacob DJ, Liao H, Shen L, Zhang Q, Bates KH. Anthropogenic drivers of
380 2013–2017 trends in summer surface ozone in China. *Proc National Acad Sci* 2019,
381 **116**(2)**:** 422-427.
382 20. Chinese State Council, Three-Year Action Plan on Defending the Blue Sky 2018,
383 **http://english.mee.gov.cn/News_service/news_release/201807/t20180713_446624.shtml**.
384

21. Kirchner F, Jeanneret F, Clappier A, Krüger B, van den Bergh H, Calpini B. Total VOC reactivity in the planetary boundary layer: 2. A new indicator for determining the sensitivity of the ozone production to VOC and NO x. *J Geophys Res-Atmos* 2001, **106**(D3)**:** 3095-3110.

22. Sillman S, Logan JA, Wofsy SC. The sensitivity of ozone to nitrogen oxides and hydrocarbons in regional ozone episodes. *J Geophys Res-Atmos* 1990, **95**(D2)**:** 1837-1851.

23. Edwards PM, Brown SS, Roberts JM, Ahmadov R, Banta RM, deGouw JA*, et al.* High winter ozone pollution from carbonyl photolysis in an oil and gas basin. *Nature* 2014, **514**(7522)**:** 351-354.

24. Sheehy PM, Volkamer R, Molina LT, Molina MJ. Oxidative capacity of the Mexico City atmosphere - Part 2: A ROx radical cycling perspective. *Atmos Chem Phys* 2010, **10**(14)**:** 6993-7008.

25. Jenkin M, Saunders S, Wagner V, Pilling M. Protocol for the development of the Master Chemical Mechanism, MCM v3 (Part B): tropospheric degradation of aromatic volatile organic compounds. *Atmos Chem Phys* 2003, **3**(1)**:** 181-193.

26. Womack CC, McDuffie EE, Edwards PM, Bares R, de Gouw JA, Docherty KS*, et al.* An Odd Oxygen Framework for Wintertime Ammonium Nitrate Aerosol Pollution in Urban Areas: NOx and VOC Control as Mitigation Strategies. *Geophys Res Lett* 2019, **46**(9)**:** 4971-4979.

27. Liu YJ, Seco R, Kim S, Guenther AB, Goldstein AH, Keutsch FN*, et al.* Isoprene photo-oxidation products quantify the effect of pollution on hydroxyl radicals over

Amazonia. *Sci Adv* 2018, **4**(4)**:** 8.

28. Barket DJ, Grossenbacher JW, Hurst JM, Shepson PB, Olszyna K, Thornberry T*, et al.* A study of the NOx dependence of isoprene oxidation. *J Geophys Res-Atmos* 2004, **109**(D11)**:** 12.

29. Wang W, Li X, Shao M, Hu M, Zeng L, Wu Y*, et al.* The impact of aerosols on photolysis frequencies and ozone production in Beijing during the 4-year period 2012–2015. *Atmos Chem Phys* 2019, **19**(14)**:** 9413-9429.

30. Jacob DJ. Heterogeneous chemistry and tropospheric ozone. *Atmos Environ* 2000, **34**(12-14)**:** 2131-2159.

31. Kleinman LI, Daum PH, Lee JH, Lee YN, Nunnermacker LJ, Springston SR*, et al.* Dependence of ozone production on NO and hydrocarbons in the troposphere. *Geophys Res Lett* 1997, **24**(18)**:** 2299-2302.

32. Tonnesen GS, Dennis RL. Analysis of radical propagation efficiency to assess ozone sensitivity to hydrocarbons and NOx: 1. Local indicators of instantaneous odd oxygen production sensitivity. *J Geophys Res-Atmos* 2000, **105**(D7)**:** 9213-9225.

33. Volkamer R, Sheehy P, Molina LT, Molina MJ. Oxidative capacity of the Mexico City atmosphere - Part 1: A radical source perspective. *Atmos Chem Phys* 2010, **10**(14)**:** 6969-6991.

34. Mao J, Ren X, Chen S, Brune WH, Chen Z, Martinez M*, et al.* Atmospheric oxidation capacity in the summer of Houston 2006: Comparison with summer measurements in other metropolitan studies. *Atmos Environ* 2010, **44**(33)**:** 4107-

4115.

35. Wang W, van der A R, Ding J, van Weele M, Cheng T. Spatial and temporal changes of the ozone sensitivity in China based on satellite and ground-based observations. *Atmos Chem Phys* 2021, **21**(9)**:** 7253-7269.

36. Kang M, Zhang J, Zhang H, Ying Q. On the Relevancy of Observed Ozone Increase during COVID-19 Lockdown to Summertime Ozone and PM2.5 Control Policies in China. *Environ Sci Technol Lett* 2021, **8**(4)**:** 289-294.

Methods

M1 Measurements

Field measurements were performed at an urban site in Beijing, August between 2006 and 2020. The site (39.99° N, 116.31°E) is located on the roof of a six-story building (~ 20 m above the ground level) on the campus of Peking University (PKUERS). Ozone (O_3) nitric oxide (NO) nitrogen dioxide (NO_2), sulfur dioxide (SO_2), carbon monoxide (CO), VOCs, aerosol optical properties, aerosol surface area concentration (S_a), photolysis frequencies of O_3, NO_2, HONO and formaldehyde (HCHO) and meteorological factors including temperature, relative humidity, wind speed, wind direction and air pressure were measured during the study period. VOCs include nonmethane hydrocarbons (NMHCs) with 56 species and C2-C6 OVOCs. For all these gas pollutant measurements, the calibration of instruments was regularly conducted. The measurement techniques are summarized in the Extended data Table 1. In addition, OMI tropospheric NO_2 columns and HCHO columns were also used for analysis (see details in Supplementary S1). Planetary boundary layer height in Beijing was obtained from the NOAA Air Resource Laboratory website (https://ready.arl.noaa.gov/READYamet.php).

Figure S1 shows a comparison between the PKUERS site and the other 12 sites from the national monitoring network (NMN) in Beijing (https://quotsoft.net/air/, NMN data available from 2014). The O_3 concentration exhibits very similar trends at the PKUERS site and the NMN sites. We have also looked at the O_3 precursor NO_2 (VOC

475 measurements are not available at the NMN sites), which exhibits also similar
476 decreasing trends at both the NMN sites and the PKUERS site. These results show that
477 data from the PKUERS site can represent the long-term trends of both O_3 and its
478 precursor NO_2 in Beijing.

479 In addition to data set in Beijing, data collected at sites in Shanghai and Hong
480 Kong were also used for additional support. Field measurements of trace gases (O_3,
481 VOCs, NO_X, CO, SO_2,), aerosols, photolysis frequencies and meteorological
482 parameters were performed at typical urban sites in Shanghai between 2011 and 2019
483 and Hongkong between 2013 and 2019. Relevant measurement data were analyzed for
484 comparison with Beijing. For all analysis, we eliminated the days with abnormally high
485 cloud optical depth when O_3 concentrations were extremely low.

486 **M2 Multiple linear regression**

487 We applied a multiple linear regression (MLR) method to quantify the effect of
488 meteorological and other physical factors on O_3:

489 $$[O_3] = \beta_0 + \sum_{i=1}^{n} \beta_i X_i + \text{interaction terms} \quad (1)$$

490 $$\text{interaction terms} = \sum \beta_{i,j} X_i X_j, \text{ for } 1 \le i, j \le n, \quad (2)$$

491 where $[O_3]$ is the daily MDA8 O_3 concentration and (X_1, ..., X_n) are major
492 meteorological and physical variables. The interaction terms are up to second order,
493 including both X_i^2 and $X_i X_{j \neq i}$. Similar MLR methods have been successfully applied to
494 quantify the effect of meteorological variability on air pollutants in North America,
495 Europe, and China[19, 37, 38]. Seven variables (j(O^1D), temperature, relative humidity,
496 wind speed, wind direction, air pressure and boundary layer height) are candidates for

497 the regression. According to the fitting test, j(O^1D), temperature, relative humidity,
498 wind speed and wind direction are more important than air pressure and boundary layer
499 height in determining the coefficient of determination (R^2). Accordingly, the five
500 dominant meteorological variables were selected for the regression. The lag terms (i.e.,
501 the effect of July conditions on August ozone) have a small effect on R^2, thus they were
502 not considered in this study.

503 Hourly values of O_3 were used to calculate daily MDA8 O_3 concentrations, and
504 hourly values of meteorological factors were averaged to daily averages. Daily averages
505 of the five dominant meteorological variables were regressed onto daily MDA8 O_3
506 concentrations to fit the effect of meteorological variability on O_3. The coefficient of
507 determination (R^2) for the MLR model is 0.65. Then the fitting results were averaged
508 to acquire the monthly O_3 anomaly of each year induced by meteorological variability.
509 The effect of meteorological factors on O_3 can be normalized by subtracting the
510 monthly O_3 anomaly from observed monthly O_3 concentrations.

511 Notably, the decreases of $PM_{2.5}$ over this 15-year period resulted in increases of
512 actinic flux and photolysis frequencies (**Fig. S2 and Fig. S5**), which could increase O_3
513 production [11, 29]. According to the model simulation of Wang et al [11], the rapid increase
514 in actinic flux causes an increase in MDA8 O_3 by 1.6 ppbv (2.3%) yr^{-1} during 2006-
515 2014, accounting for 66% of the increase in O_3 concentrations during this period. In
516 this study, we aim to explore emission control strategy for O_3 mitigation by
517 investigating the relationship between O_3 trend and precursor trend. In this case, we
518 must remove the effect of the change in photolysis frequencies on the O_3 trend by the

519 normalization of j(O^1D), which helps to show a clearer relationship between O_3 trend
520 and precursor trend.

521 **M3 Model simulation**

522 The photochemistry of radicals and ozone in Beijing were studied by using a zero-
523 dimension photochemical box model. Previous studies indicate that the variation in
524 ozone concentrations at PKUERS site was mainly influenced by local photochemistry,
525 and background ozone contributed < 30% of the variation in ozone concentrations [11, 12].
526 In this case, box model is suitable for studying the photochemistry of ozone and OH
527 radicals at PKUERS site. The box model has the advantage of allowing detailed
528 treatment of the VOC oxidation chemistry, at the expense of a comprehensive
529 representation of dynamical processes.

530 The photochemical box model uses the Master Chemical Mechanism (MCM)
531 v3.3.1 as chemical mechanism [39]. The MCMv3.3.1 chemistry scheme contains 5832
532 species and 17224 reactions, which can accurately simulate the radical source,
533 conversion and termination to understand the O_3 formation. Model calculations are
534 constrained to measured meteorological factors (i.e., photolysis frequencies,
535 temperature, relative humidity and air pressure), inorganic species (NO, NO_2, CO, O_3
536 and SO_2), NMHCs and aerosol surface area concentrations. The OVOC species that
537 were continuously measured during the 15 years including acetaldehyde, acetone,
538 methyl ethyl ketone, MVK and MACR were constrained in the model. HCHO was not
539 constrained in the model due to the limitation of measurement data and thus was

simulated by the model. To consider the contribution of primary emissions to HCHO, we set emission rates of HCHO in Beijing in the model (3.3-11.5×10^{-12} kg m^{-2} s^{-1}), which is derived from local emission inventories - the MEIC inventory (http://www.meicmodel.org/). To evaluate the model performance, the model-simulated HCHO was compared with observations in August 2008, 2011 and 2012, which shows a difference of 14% for daytime averages (Fig. S10). This difference is smaller than the uncertainty of model simulation (30%) associated with the uncertainty of various measurement parameters, reaction rate constants and emission rates of HCHO (Supplementary S7), suggesting a good performance of the model in the simulation of HCHO. The five constrained OVOCs and HCHO totally contribute >65% of total $OVOC^R$ and >70% of total $P(RO_X)$ from OVOC photolysis (Fig. S11).

The model runs were performed in a time-dependent mode with a 1-hour resolution. A whole month (August) of each year was simulated with three days' spin-up. The diurnal variation in boundary layer height was expressed as a dilution term in the box model to represent the physical losses. The convection of O_3 between near surface air and the residual layer aloft was considered in the box model, according to the method of Womack et al. [26]. The dry deposition rate for O_3 was set as 0.42 cm s^{-1} in the daytime and 0.14 cm s^{-1} in the nighttime, as the deposition rate is known to decrease after sunset [26, 40, 41]. To account for background O_3 transported from outside the investigated cities, we set the background O_3 of 35 ppbv, which are derived from observed O_3 concentrations at regional background sites in China [42]. For other species such as radicals and OVOCs, the concentrations mixed into the box was set as zero

because of their short lifetime.

Aerosols can influence O_3 production by heterogeneous reactions such as uptake of HO_2, N_2O_5, NO_2 and NO_3. This includes the uptake coefficients are 0.08 for conversion of HO_2 to H_2O [43], 0.007 for conversion of N_2O_5 to HNO_3 [44], 2×10^{-5} for conversion of NO_2 to HONO and HNO_3 (which yields a good simulation of $HONO/NO_2$ concentration ratios in Beijing [45]) and 1×10^{-3} for conversion of NO_3 to HNO_3 [30].

Direct measurements of OH concentration were not made during the study period; hence, we simulated OH concentrations by the box model. To identify the primary causes of the continuous OH increase from 2006 to 2020, we performed sensitivity analyses of the relevant factors. The investigated factors include photolysis frequencies, NO_X, VOCs, aerosol uptake and other factors including O_3, H_2O and temperature. We take the simulation result in 2006 as the base scenario. For the testing scenario, we set one of investigated factors to the level of 2020, with other conditions fixed to levels of 2006. The difference in simulated OH concentrations between the base scenario and the testing scenario represents the effect of this investigated factor on the OH increase. Notably the effect of aerosol uptake is quantified by changing aerosol surface area concentrations in the model. Similar sensitivity analysis method has been applied by Li et al. [19]

Due to the limitation of measurement data, some important OVOCs are not constrained in the model such as acrolein, n-butanal, n-hexanal, n-pentanal, propanal, pentanone, methanol and C7-C10 OVOCs. We investigated the impact of whether these

584 OVOCs are constrained in the model or not on our analysis. The model simulation
585 focuses on August 2017 when these OVOCs were measured. As shown in Fig. S14,
586 daytime averages of O_3 concentrations, $P(O_3)$, $P(RO_X)$ and ChL changed by 10%, 17%
587 and 12% and 11% between the two scenarios, indicating that our modelling setup
588 without these OVOCs constrained is acceptable for the analysis of this study although
589 some bias exists. Even though, the impact of these unconstrained OVOCs on O_3
590 production and trends cannot be ignored, which should be paid more attention to in the
591 future. In addition, other important photodegradable OVOCs that were not measured
592 such as peroxyacetic acid and pyruvic acid may also cause bias.

593 **M4 Calculation of $P(O_3)$, $P(RO_X)$, ChL and total OH turnover rate**

594 The dominant chemical source of O_3 in the troposphere is the reaction of OH with
595 VOCs to produce peroxyl radicals (HO_2 and RO_2), which then react with NO to yield
596 NO_2 [46]. The overall process can be summarized as:

597 $$OH + VOC \rightarrow RO_2 \ \ or \ \ HO_2 \quad (R1)$$

598 $$RO_2 + NO \rightarrow \ \ HO_2 + NO_2 \quad (R2)$$

599 $$HO_2 + NO \rightarrow \ \ OH + NO_2 \quad (R3)$$

600 $$NO_2 + O_2 + h\nu \rightarrow \ \ O_3 + NO \quad (R4)$$

601 The ozone production rate ($P(O_3)$) is equal to the reaction rate of peroxyl radicals
602 with NO (i.e., sum of rates of R2 and R3):

603 $$P(O_3) = k_{HO2+NO}[HO_2][NO] + \sum_i (k^i_{RO2+NO}\left[RO^i_2\right][NO]) \quad (3)$$

604 By defining an average reaction rate constant for all RO_2+NO reactions, k_{RO2+NO},
605 we obtain:

$$P(O_3) = k_{HO2+NO}[\mathrm{HO_2}][\mathrm{NO}] + k_{RO2+NO}[\mathrm{RO_2}][\mathrm{NO}] \quad (4)$$

Our model indicates that k_{RO2+NO} was in the range of 8.45–9.58×10^{-12} cm^3 molecule^{-1} s^{-1} in Beijing 2006-2020, which was close to k_{HO2+NO} value (8.45×10^{-12} cm^3 molecule^{-1} s^{-1}). Thus:

$$P(O_3) \approx k_{HO2+NO}([\mathrm{HO_2}][\mathrm{NO}] + [\mathrm{RO_2}][\mathrm{NO}]) = \alpha k_{HO2+NO}[\mathrm{HO_2}][\mathrm{NO}] \quad (5)$$

$$\alpha = ([\mathrm{HO_2}] + [\mathrm{RO_2}])/[\mathrm{HO_2}] \quad (6)$$

The model simulation indicates that the $\alpha \approx 1.8$ in Beijing, which remained approximately constant over the 2006-2020 period. The uncertainty in various measurement parameters and reaction rate constants leads to 22% uncertainty of α (Supplementary S7). To test the effect of un-included OVOCs with larger carbon number on α, we increased C7-C10 OVOCs by 0.68 ppb (the observed value in 2017) in the model, resulting in an increase of α by 5%.

ChL characterizes the number of iterations each RO_X radical makes prior to termination, and is the ratio of OH cycling rate (i.e., the rate of reaction R3) to radical primary production rate ($P(RO_X)$). ChL depends on the levels of VOCs and NO_X with modest impact from actinic flux.

$$\mathrm{ChL} = \alpha \frac{k_{HO2+NO}[\mathrm{HO_2}][\mathrm{NO}]}{\mathrm{P(RO_X)}} \quad (7)$$

The primary production of the peroxyl radicals, $P(RO_X)$, is determined by the photolysis of radical precursors (including carbonyls, nitrous acid and O_3) and alkene ozonolysis; these are the radical chain initiation reactions:

$$P(RO_X) = 2 \times [\mathrm{O_3}] \times j(O^1D) \times \theta + [\mathrm{HONO}] \times j(HONO) + \sum_i([\mathrm{OVOC_i}] \times j_i \times \gamma_i) + \text{alkene ozonolysis} \quad (8)$$

where θ is the fraction of O^1D from ozone photolysis that reacts with H_2O. $OVOC_i$

represents each OVOCs species, j_i represents the photolysis frequency of each $OVOC_i$, and γ_i represents the number of ROX radicals generated from the photolysis of each $OVOC_i$ molecule. For most OVOCs species, γ_i is equal to 2 or 0.

When the radial chain cycling is much more important than chain initiation (or equivalently, chain termination), i.e., ChL >>1, R1 and R3 dominate the source and sink of peroxy radicals (HO_2 and RO_2), respectively. In this case, the reaction rates of R1 and R3 are approximately equal given the short lifetime of peroxy radicals (~ several minutes). **Extended data Fig. 5** shows that $k_{HO2+NO}[HO_2][NO]:[OH]\times VOC_R$ gets closer to 1:1 as ChL increases to 5. In Beijing, the ChL was in the range of 4.3~5.4 (**Fig. 3A**). Under this condition, the reaction rates of R1 and R3 were approximately equal:

$$P(O_3) = \alpha k_{HO2+NO}[HO_2][NO]$$

$$= \alpha k_{OH+VOC}[OH][VOC] = \alpha[OH]VOC_R \quad (9)$$

The total OH turnover rate is the total reaction rate of all reactive species with OH radical:

$$Total\ OH\ turnover\ rate = [OH]\times\sum_j k_{OH+S_j}[S_j] \quad (10)$$

$\sum_j k_{OH+S_j} S_j$ is the total OH reactivity of all reactive species including VOCs, NOX, SO_2 and CO. S_j represents each reactivity species. k_{OH+S_j} is the reaction rate coefficient for the reaction between reactive species S_j and OH. The total OH turnover rate characterizes the rate of secondary production (including ozone and secondary aerosols) induced by OH, which closely relates to the level of secondary pollution.

O_3 precursor sensitivity depends on the dominant loss pathways of ROX radicals. O_3 production is NOX-limited if the self-reaction of peroxyl radicals dominates the ROX

653 sink, and VOC-limited if the reaction of NO_2 with OH dominates[31, 46]. Accordingly, the
654 ratio of OH+NO_2 reaction rate to the total rates of the two RO_X sinks, i.e., L_N/Q, is used
655 to identify O_3 sensitivity regimes. O_3 production is NO_X-limited if L_N/Q is lower than
656 0.5, otherwise, it is VOC-limited or NO_X-saturated [31]. As shown in Fig. S15, L_N/Q is
657 larger than 0.5 from 2006 to 2020, indicating a NO_X-saturated regime.

658 $$L_N/Q = \frac{k_{OH+NO_2}[OH][NO_2]}{k_{HO_2+RO_2}[HO_2][RO_2]+k_{HO_2+HO_2}[HO_2][HO_2]+k_{OH+NO_2}[OH][NO_2]} \quad (11)$$

659

Data availability

The data and code to generate the results in the manuscript are freely available at Open Research Data Repository of the Max Planck Society (https://doi.org/10.17617/3.LEFS4A).

Code availability

The box model is available from https://sites.google.com/site/wolfegm/models.

Methods-only References

37. Otero N, Sillmann J, Mar KA, Rust HW, Solberg S, Andersson C*, et al.* A multi-model comparison of meteorological drivers of surface ozone over Europe. *Atmos Chem Phys* 2018, **18**(16)**:** 12269-12288.

38. Tai APK, Mickley LJ, Jacob DJ. Correlations between fine particulate matter (PM2.5) and meteorological variables in the United States: Implications for the sensitivity of PM2.5 to climate change. *Atmos Environ* 2010, **44**(32)**:** 3976-3984.

39. Wolfe GM, Marvin MR, Roberts SJ, Travis KR, Liao J. The framework for 0-D atmospheric modeling (F0AM) v3. 1. *Geosci Model Dev* 2016, **9**(9)**:** 3309.

40. Zhang L, Brook JR, Vet R. A revised parameterization for gaseous dry deposition in air-quality models. *Atmos Chem Phys* 2003, **3:** 2067-2082.

41. Yang S, Yuan B, Peng Y, Huang S, Chen W, Hu W*, et al.* The formation and mitigation of nitrate pollution: comparison between urban and suburban environments. *Atmos Chem Phys* 2022, **22**(7)**:** 4539-4556.

42. Xu X, Lin W, Xu W, Jin J, Wang Y, Zhang G*, et al.* Long-term changes of regional ozone in China: implications for human health and ecosystem impacts. *Elem Sci Anth* 2020, **8**.

43. Tan Z, Hofzumahaus A, Lu K, Brown SS, Holland F, Huey LG*, et al.* No Evidence for a Significant Impact of Heterogeneous Chemistry on Radical Concentrations in the North China Plain in Summer 2014. *Environ Sci Technol* 2020, **54**(10)**:** 5973-5979.

44. Wang H, Lu K, Tan Z, Sun K, Li X, Hu M*, et al.* Model simulation of NO3, N2O5 and ClNO2 at a rural site in Beijing during CAREBeijing-2006. *Atmos Res* 2017, **196:** 97-107.

45. Hendrick F, Muller JF, Clemer K, Wang P, De Maziere M, Fayt C*, et al.* Four years of ground-based MAX-DOAS observations of HONO and NO2 in the Beijing area. *Atmospheric Chemistry and Physics* 2014, **14**(2)**:** 765-781.

46. Kleinman LI. The dependence of tropospheric ozone production rate on ozone precursors. *Atmos Environ* 2005, **39**(3)**:** 575-586.

696

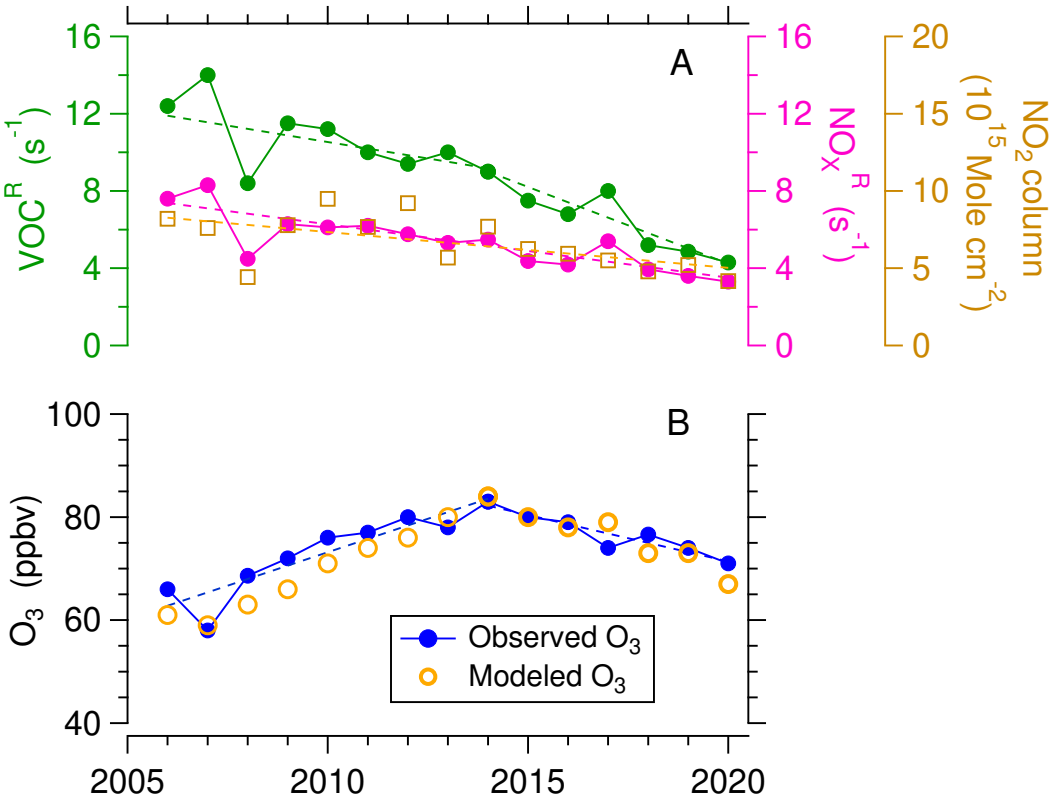
A
16
12
8
4
0
VOC^R (s^-1)
16
12
8
4
0
NOx^R (s^-1)
20
15
10
5
0
NO2 column (10^15 Mole cm^-2)

B
100
80
60
40
O3 (ppbv)
2005
2010
2015
2020
Observed O3
Modeled O3

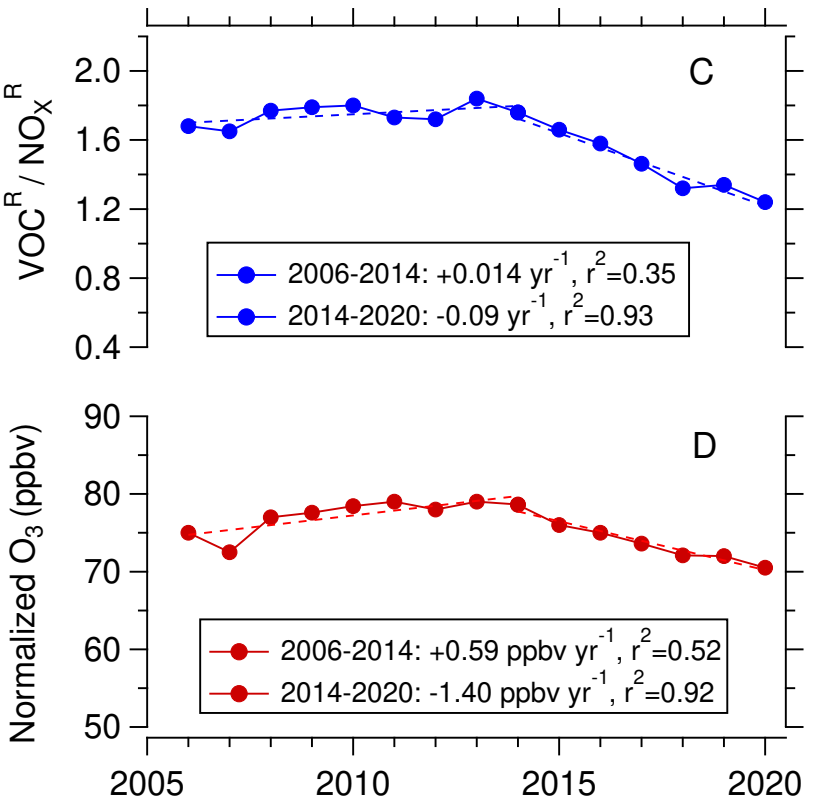
C
2.0
1.6
1.2
0.8
0.4
VOC^R / NOx^R
2006-2014: +0.014 yr^-1, r^2=0.35
2014-2020: -0.09 yr^-1, r^2=0.93

D
90
80
70
60
50
Normalized O3 (ppbv)
2005
2010
2015
2020
2006-2014: +0.59 ppbv yr^-1, r^2=0.52
2014-2020: -1.40 ppbv yr^-1, r^2=0.92

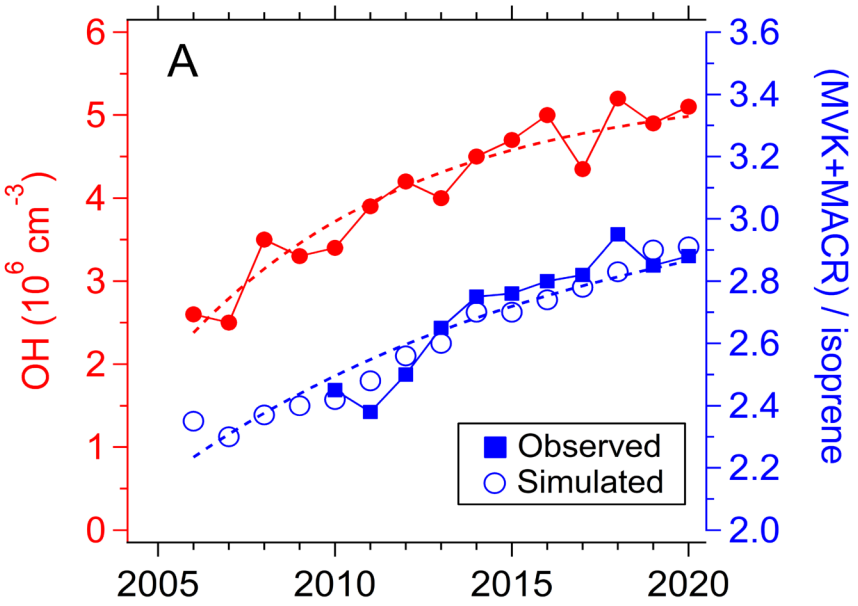
A
OH (10^6 cm^{-3})
(MVK+MACR) / isoprene
Observed
Simulated
2005
2010
2015
2020

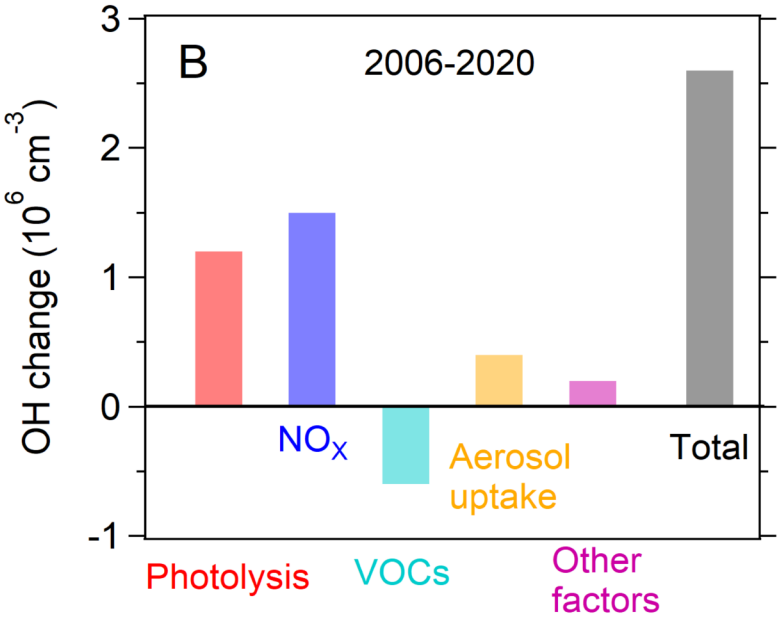
B
2006-2020
OH change (10^6 cm^{-3})
NO_X
Aerosol uptake
Total
Photolysis
VOCs
Other factors

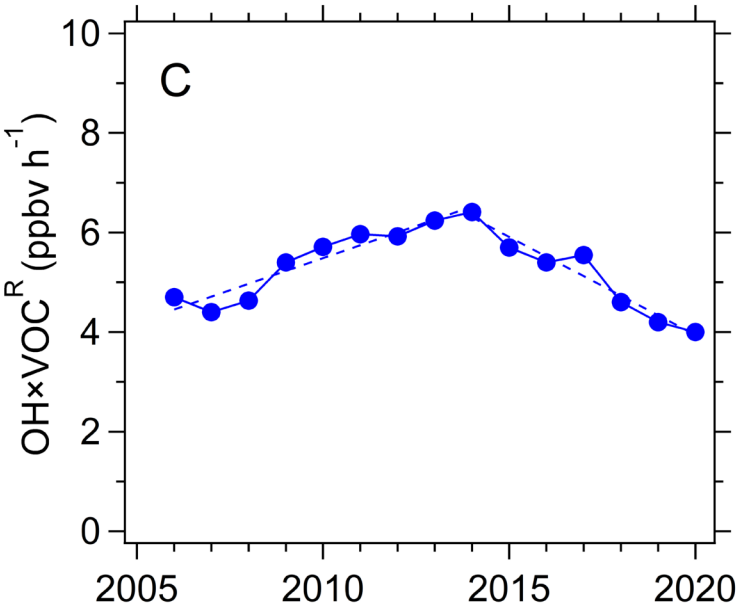
C
OH×VOC^R (ppbv h^{-1})
2005
2010
2015
2020

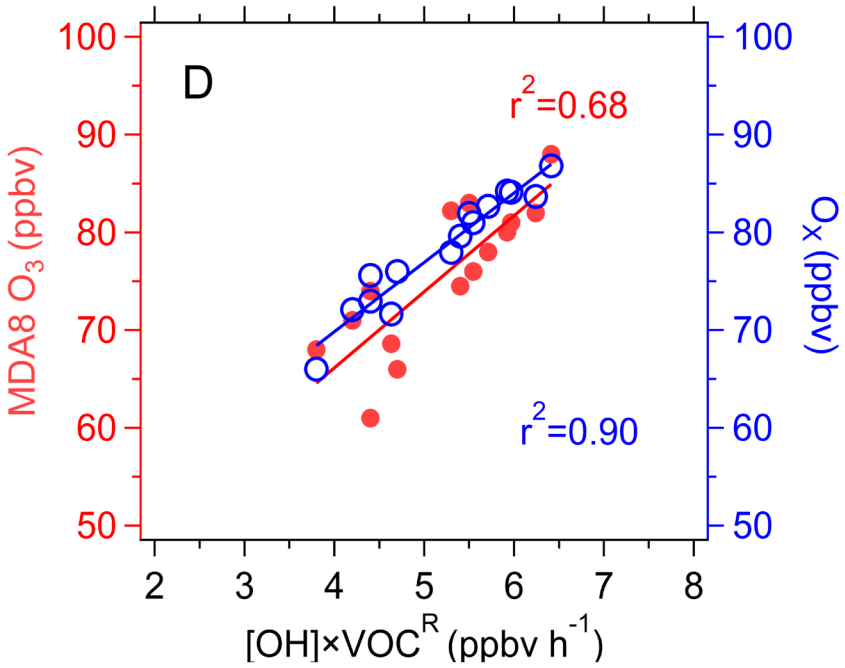
D
r^2=0.68
r^2=0.90
MDA8 O_3 (ppbv)
O_X (ppbv)
[OH]×VOC^R (ppbv h^{-1})

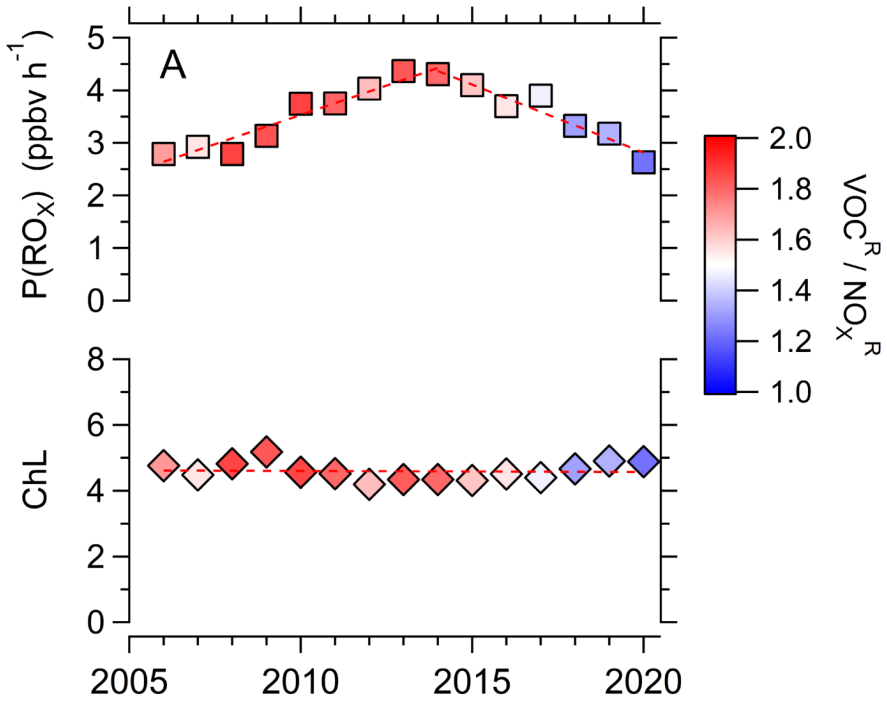
A
P(ROX) (ppbv h-1)
ChL
VOCR / NOXR
2.0
1.8
1.6
1.4
1.2
1.0
2005
2010
2015
2020

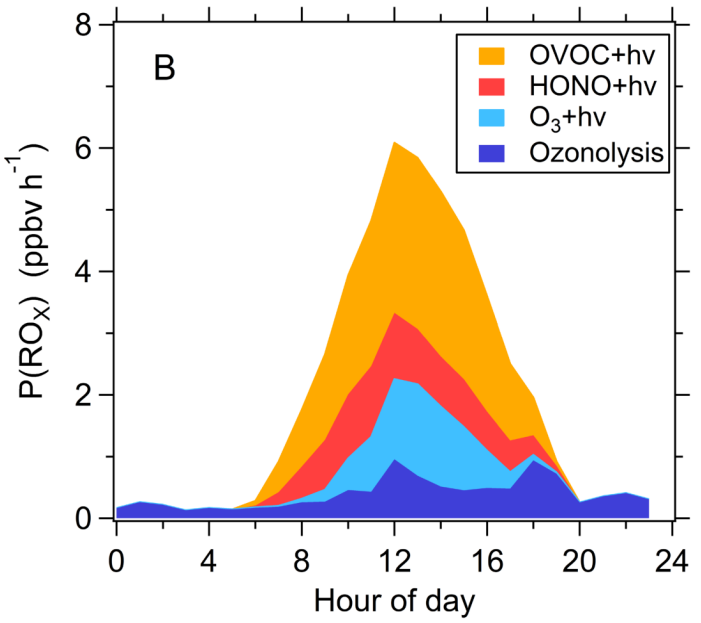
B
OVOC+hv
HONO+hv
O3+hv
Ozonolysis
P(ROX) (ppbv h-1)
Hour of day

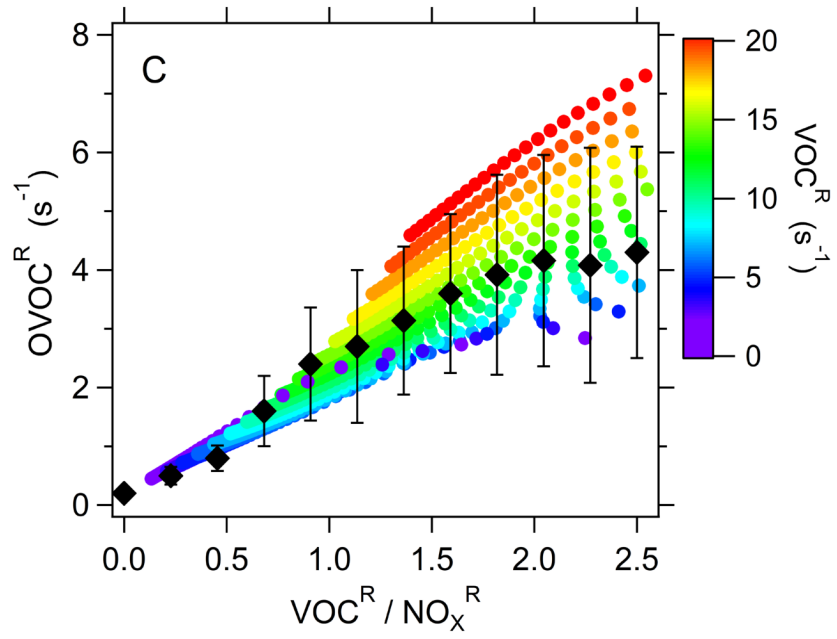
C
OVOCR (s-1)
VOCR / NOXR
VOCR (s-1)

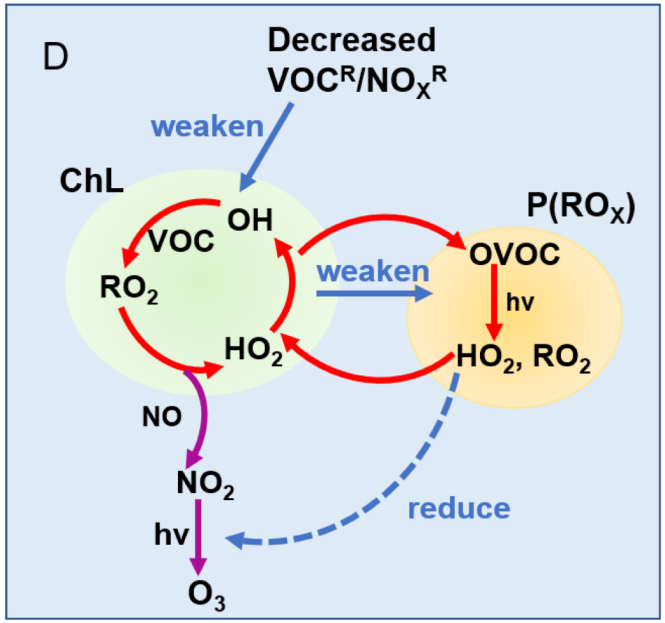
D
Decreased
VOCR/NOXR
weaken
ChL
OH
VOC
RO2
HO2
weaken
P(ROX)
OVOC
hv
HO2, RO2
NO
NO2
hv
O3
reduce

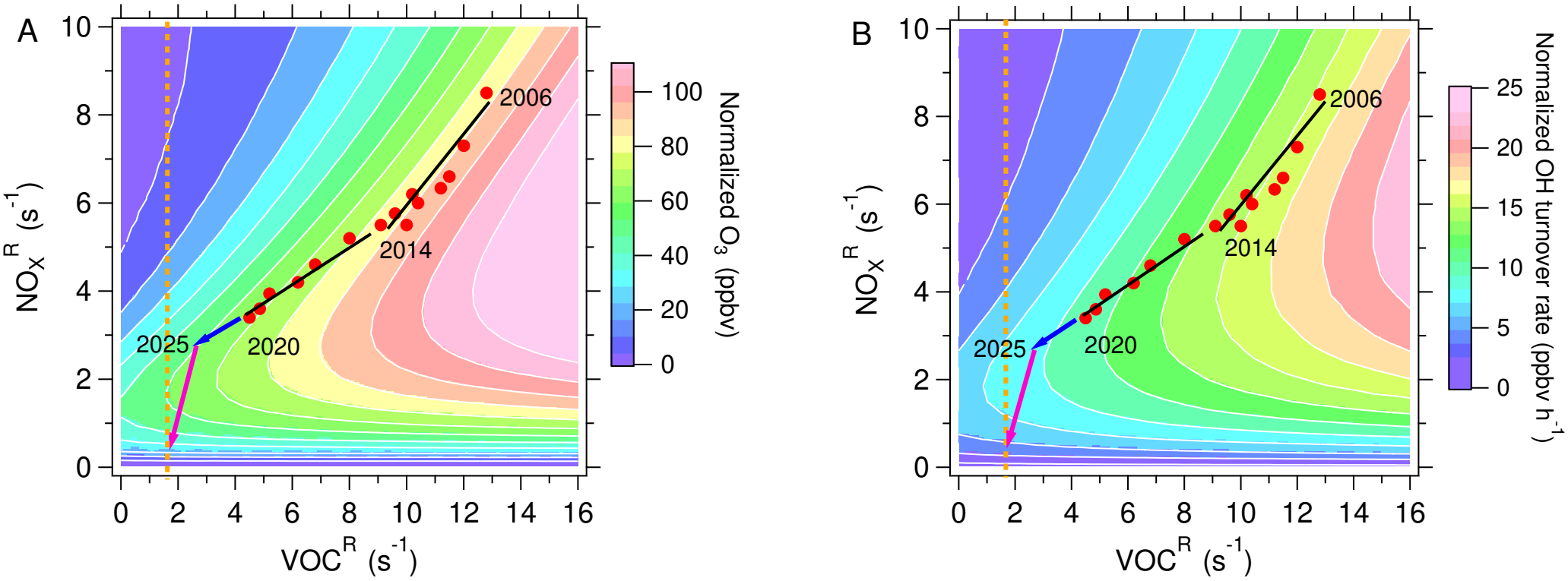
A
B
2006
2014
2020
2025
NO_X^R (s^{-1})
VOC^R (s^{-1})
Normalized O_3 (ppbv)
Normalized OH turnover rate (ppbv h^{-1})